Understanding Electrocatalytic Pathways in Low and Medium Temperature Fuel Cells: Synchrotron-based *In Situ* X-Ray Absorption Spectroscopy

by Sanjeev Mukerjee, Joseph Ziegelbauer, Thomas Arruda, David Ramaker, and Badri Shyam

Over the last few decades, researchers have made significant developments in producing more advanced electrocatalytic materials for power generation applications. For example, traditional fuel cell catalysts often involve high-priced precious metals such as Pt. However, in order for fuel cells to become commercially viable, there is a need to reduce or completely remove precious metal altogether. As a result, a myriad of novel, unconventional materials have been explored such as chalcogenides, porphyrins, and organic-metal-macrocycles for low/medium temperature fuel cells as well as enzymatic and microbial fuel cells.[1-3] As these materials increasingly become more complex, researchers often find themselves in search of new characterization methods, especially those which are allow *in situ* and *operando* measurements with element specificity.

One such method that has received much attention for analysis of electrocatalytic materials is X-ray absorption spectroscopy (XAS). XAS is an element specific, core level absorption technique which yields structural and electronic information. As a core electron method, XAS requires an extremely bright source, hence a synchrotron. The resulting intensity of synchrotron radiation allow for experiments to be conducted *in situ*, under electrochemically relevant conditions. Although a bulk-averaging technique requiring rigorous mathematical manipulation, XAS has the added benefit that it can probe materials which possess no long range order. This makes it ideal to characterize nano-scale electrocatalysts.

XAS experiments are conducted by ramping the X-ray photon energy while measuring absorption of the incident beam the sample or by counting fluorescent photons released from a sample due to subsequent relaxation. Absorption mode XAS follows the Beer-Lambert Law,

$$\mu x = \log(I_0/I_t) \qquad (1)$$

where μ is the absorption coefficient, x is the sample thickness and I_0 and I_t are the intensities of the incident and transmission beams respectively. When the energy of the incident X-rays exceed the electron binding energy (E_0) of the element under investigation, the electron is ejected from the core to available excited states in the form of a photoelectron with kinetic energy:

$$E_k = h\nu - E_0 \qquad (2)$$

with, E_k being the kinetic energy of the released photoelectron and $h\nu$ the energy of the incident beam.

In general, the X-ray absorption spectrum is broken down into two distinct energy regions: the X-ray absorption near-edge structure or XANES ($-50eV \leq E_0 \leq 50eV$) and the extended X-ray absorption fine-structure or EXAFS ($50eV \leq E_0 \leq \sim1000eV$). The XANES region is dominated by low-energy photoelectrons which undergo multiple scattering events. As such, it can reveal information about oxidation state, local symmetry, electronic structure, and the extent of oxidation of a material. Due to this complex multiple scattering, there is no simple XANES equation to describe it quantitatively. However, recent advancements in computers and the evolution of numerical methods such as the FEFF code[4] have made possible reliable XANES simulations.

Photoelectrons in the EXAFS region have high enough E_k to undergo primarily single back-scattering events. These back-scattered photoelectrons interfere with the outgoing photoelectrons, causing the oscillations in the absorption spectrum. Using the previously developed EXAFS equations[5] it is now possible to model EXAFS data to determine coordination numbers, bond distances, and mean-square disorder (commonly referred to as Debye-Waller factor). EXAFS data is often shown by Fourier Transforming K-Space into distance, r, space where the total magnitude is plotted against the radial coordinates. This allow for easy qualitative comparison of samples. Employing EXAFS on nano-scale materials has the added advantage that it can quantitatively illustrate changes in atom-atom coordination, which can be related to particle size or morphology.

Overall this technique enables the measurement of both bulk and surface adsorbed species with element specificity under actual electrochemical operating conditions. Thus this represents the one of the most powerful methods to understand the exact role of the reaction center and degradation processes such as sintering and corrosion.

Conventional XAS in Electrocatalysis

XAS measurements on powder materials and liquids are easily made by a variety of methods. Typically, powder samples are measured out for the correct XAS loading (calculated on the basis of theoretical absorption cross section in transmission and fluorescence modes) and prepared for XAS by pressing into pellet form and placed into the beam path. *In situ* work however, typically requires a more sophisticated sample holder. Many *in situ* spectro-electrochemical cell designs have been employed and depend on their application. Several of such cells are shown in a recent review article by Russell, *et al*.[6] Most designs involve an X-ray window in which some variety of membrane electrode assembly (MEA) is placed with a very small electrolyte layer to minimize beam attenuation. The setup in a typical three electrode mode including a reference (typically a sealed or dynamic hydrogen electrode) is connected to a potentiostat/galvanostat so that the catalyst could be characterized under actual electrochemical operating conditions. One such rendition used recently is shown in Fig. 1; this is a modification of our previous transmission XAS cell design.[7-9] The modified cell design enables the acquisition of fluorescence, total electron yield as well as transmission data.

Early on, both XANES and EXAFS gained popularity in electrocatalysis for its ability to probe fuel cell electrocatalysts particle size effects of Pt/C. The first peak in the XANES region—historically referred to as a "white line" due to its appearance on photographic plates—has been invaluable for describing the electronic state of the Pt particles. For Pt/C particles of both 1.0 and 3.7 Å, XANES white lines are observed increasing in magnitude with electrode potential.[10,11] However, white line intensities increased more in the smaller particles containing a greater fraction of surface atoms. By making measurements at both the Pt L_3 and L_2 edges ($2p_{3/2}$ and $2p_{1/2}$ respectively), and integrating the white line peaks, the percentage of unoccupied d-states have been calculated.[12] For example, the electronic effects of H and OH adsorption on Pt/C particles are more extreme on smaller particles than the larger ones
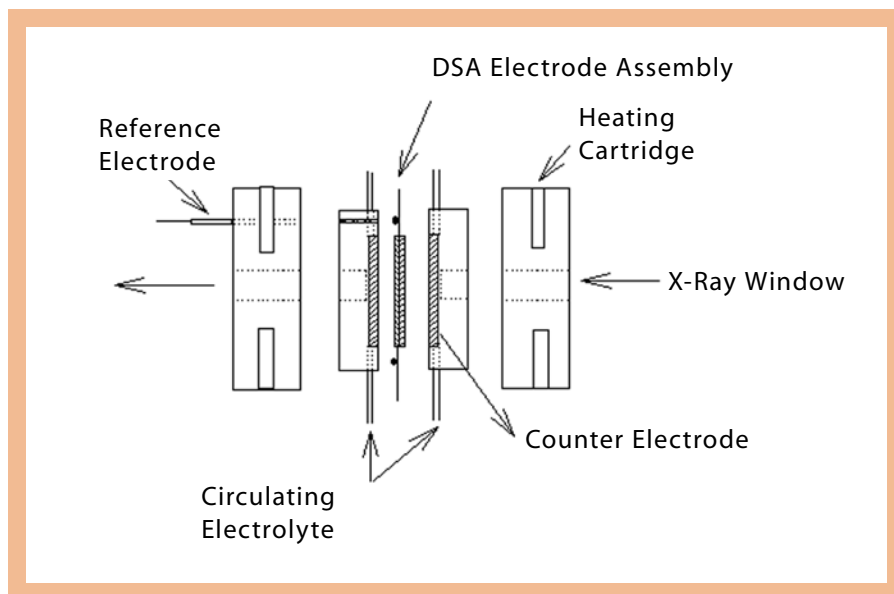
Fig. 1. *Schematic of an* in situ *spectroelectrochemical cell used for measuring data in transmission, fluorescence, and total electron yield modes. (Cell design courtesy, Prof. Eugene Smotkin and Emily Lewis, Northeastern University)*

as evidenced from the XANES. For the larger particles which exhibit a decreased OH adsorption strength, there are more surface sites available to perform the oxygen reduction reaction.[13]

Perhaps one of the most common uses for *in situ* XAS is the ability to determine average coordination number (N), particle size and shape as a function of electrode potential. As mentioned above, smaller particles have a larger fraction of their atoms at the surface. As such, changes in N with applied electrode potential are easily observed. For instance, oxide growth has been measured[14] by fitting EXAFS data taken at intervals from 0.1V up to 1.2V vs. a saturated calomel electrode (SCE). The Pt-Pt peak near 2.8 Å in the FT-EXAFS is observed decreasing, as an increasing Pt-O signal at ~1.8 Å is obtained. This is easily explained by an increase in Pt-O interactions at the expense of the Pt-Pt bonds. In the hydrogen region (~ 0 V vs. RHE), the largest N values are observed indicating a fully reduced particle. In going from 0V to 0.54V vs. RHE, N has been shown to decrease, however, with little/no oxide formation indicated in the EXAFS.[10] This has been proposed to occur by the particles transforming from spherical type geometry to a flatter one.[10]

Bi-metallic catalysts have also been explored by XAS. Although more difficult to analyze, important information has been extracted. Perhaps one of the most important bi-metallic catalysts is PtRu as it is known for possessing superior methanol/CO tolerance in comparison to Pt alone.[15] The presence of beats in the EXAFS makes the analysis complicated. These so-called beats occur because of different backscattering phase shifts from Pt and

Ru which cause destructive interference in the EXAFS.[16] First coordination shell fits for PtRu have been invaluable however, for determining the degree of alloying. Well alloyed PtRu shows Pt-Ru and Ru-Pt coordination numbers (Pt-L_3 and Ru-K edges respectively) that are in agreement.[17,18] Whereas, fits of poorly alloyed PtRu materials indicate Ru exists primarily as some form of RuO.[18]

Fuel cell durability continues to be a major obstacle in their commercialization. In particular, the direct methanol fuel cell (DMFC) has been plagued with stability issues at the PtRu anode due to Ru dissolution.[19] PtRu stability remains the subject of investigation by many investigators. As Ru leaves the surface it should be evident by a decrease in N_{Ru-Pt}, from that, for well alloyed PtRu. Many PtRu materials however, are poorly alloyed and do not show any large N_{Ru-Pt} contribution. To further complicate matters, Ru which has left the surface can be found re-deposited onto the surface or in the bulk electrolyte.[20]

New Frontiers of XAS

While the conventional XAS technique allows for the extraction of highly detailed structural and electronic information of bulk materials, XAS has traditionally been rather limited in gleaning the effective surface chemistry involved in electrocatalysis (*i.e.* weakly-bound adsorbate interactions) due to its bulk-averaging nature. This limitation has been alleviated by the "Δμ" analysis technique and atomic X-ray absorption fine-structure (AXAFS) pioneered by Koningsberger and Ramaker,[21-24] thus turning XAS into a truly surface sensitive technique. One of the greatest limi-

tations to XAS analysis, as mentioned above was the inability to accurately describe multiple scattering processes in the XANES. But as XAS gained popularity, a demand for more accurate XAS analysis became apparent. The FEFF code of Rehr and co-workers[4]—initially constructed to calculate F-effective (as the name suggests) of the EXAFS equation—has evolved to include full multiple scattering approximations. Together these have allowed significant advancements in our understanding of electrocatalysis.

Version 8.0 of the FEFF code has been, and still is used today to simulate XANES spectra. Teliska, *et al*. was first to use the novel XANES difference analysis to reveal the binding site of adsorbed hydrogen on small Pt clusters in an electrochemical environment.[25] It was noticed that carefully aligning, normalizing, and subtracting *in situ* XANES data of Pt taken in the hydrogen region produced a very specific, sinusoidal line shape in the region of the absorption edge. The theory being that the white line intensity is affected by the orbital overlap of an adsorbate. Subtracting off the XANES of a clean cluster enables the removal of contributions from the bulk (assuming the bulk does not change), and emphasizes the surface-adsorbate interaction. The total absorption signal from XAS, μ, can be described as $\mu = \mu_0(1 + \chi)$; where μ_0 represents the absorption contribution from an atom embedded in a potential well, and χ is the total EXAFS contribution. The total change in μ, Δμ, as affected by an adsorbed moiety, A, on the absorbing atom (substrate) of interest, S, can therefore be explicitly described as $\Delta\mu = \Delta\mu_0 + \Delta(\mu_0\chi_{S-S}) + \mu_0'\chi_{S-A}$, where $\Delta\mu_0$ is the change in the atomic XAFS. The Δμ technique can thus be considered a subtractive technique, and that the total effective signal can be given by the simple formalism: $\Delta\mu = \mu(S-A) - \mu(S_{clean})$. Essentially, if the bulk substrate material is not changing (*e.g.* corroding or changing phase/crystal structure as evidenced by the electrochemistry and full EXAFS spectrum analysis), careful normalization and subtraction of the XANES signals at different potentials from the clean potential (*i.e.* the double layer) will result in a spectrum that has completely eliminated the underlying chemically un-reactive bulk signal, leaving behind a spectrum that corresponds only to that part of the substrate which is covered with weakly interacting adsorbed surface species.

The resulting difference spectra obtained by the Δμ technique do not offer much information by themselves. A proper interpretation involves comparing theoretical Δμ spectra to the experimentally derived curves. By far the most popular software for constructing these theoretical spectra is the FEFF 8.0 code. FEFF performs *ab initio* self-consistent field (in real

Mukerjee, *et al.*
(continued from previous page)

space) multiple scattering calculations. To generate the theory Δμ spectrum, first a theoretical XANES spectrum of a 3-dimensional model of the clean (adsorbate-free) cluster is generated for future subtractive purposes. These models must be generated from the structural information gleaned from a full analysis of the experimental EXAFS spectrum of the material of interest in order to account for deviations from ideal (and typically unrealistic) theoretical morphologies. XANES spectra obtained by covering the afore-mentioned clean model with differing adsorbed species (at different geometries) are then normalized to, and then subtracted from, the clean theory XANES spectrum to

obtain the theoretical Δμ. Comparisons then allow for interpretation of the examined substrate in respect to electrochemical potential and adsorbate chemistry, extent, and site symmetry. We have successfully validated this technique and shown its unprecedented promise in recent publications.[26-32]

This methodology has been extended to O adsorption on Pt and Pt-M alloys At 0.7 V vs. RHE, O is seen adsorbing 1-fold (atop) on Pt, but as the potential is increased O spills over to an n-fold (n = 2,3) configuration. Above 1.0 V place exchange is observed and O is seen going sub-surface.[33,34] Previously it was believed that place exchange[35] occurred above 1.2 V. This is shown in Fig. 2. This represents a good representation of the power of this new rendition of XANES

analysis. For the first time the place exchange mechanism proposed three decades ago,[35,36] is now spectroscopically visible.

Transitioning to Non Pt Reaction Centers

The true power of this technique rests in its ability to probe more complex reaction centers which involve atoms in regular intervals within an inorganic framework structure such Rh_xS_y type chalcogenides[37] for oxygen reduction catalysis and biological mimics such as Co-tetramethyphenyl porphyrins (Co-TMPP).

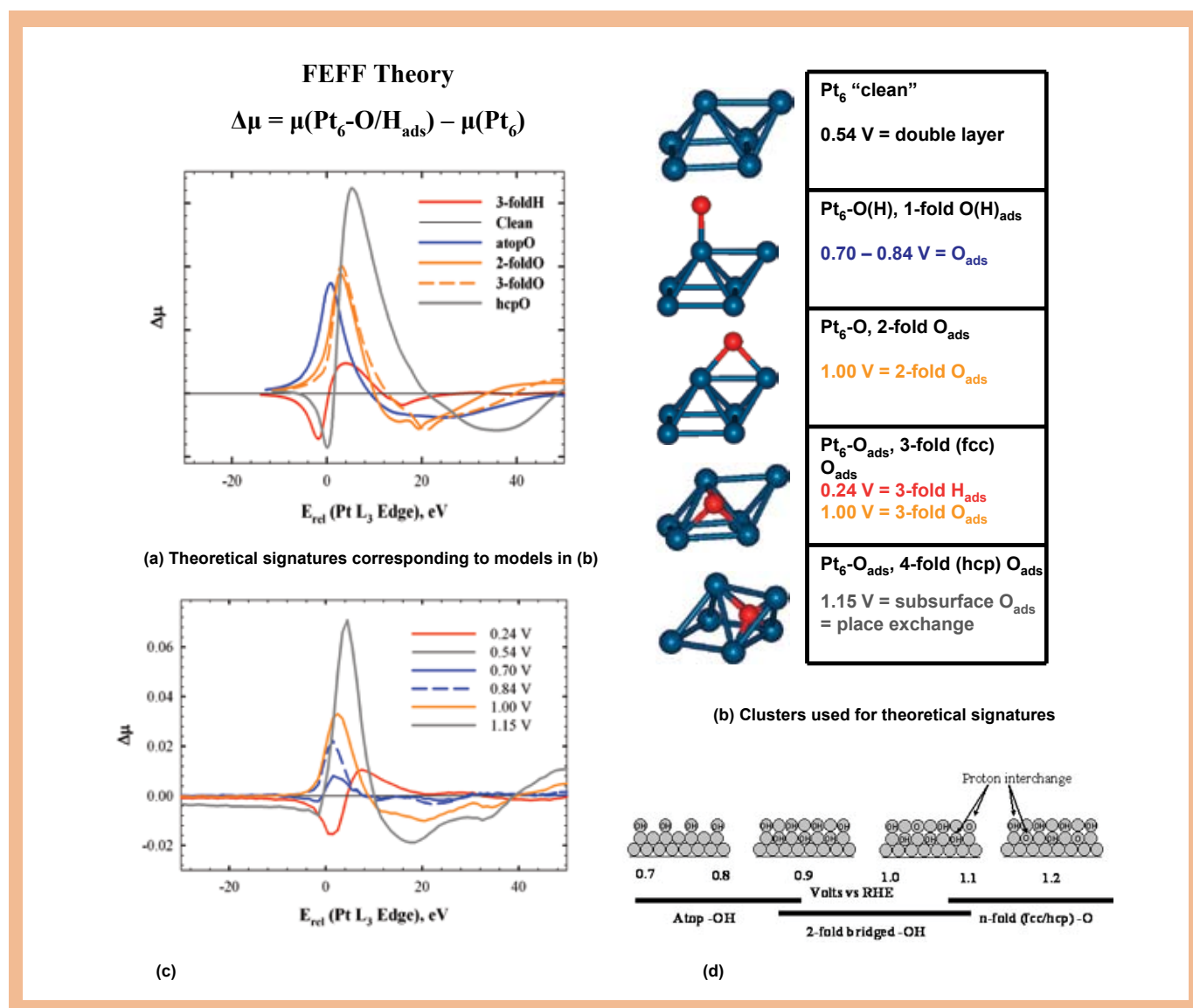***Oxygen reduction on transition metal porphyrins***.—Transition metal-based porphyrins, analogous in

FEFF Theory

$$\Delta\mu = \mu(Pt_6\text{-}O/H_{ads}) - \mu(Pt_6)$$

Legend (a): 3-foldH, Clean, atopO, 2-foldO, 3-foldO, hcpO

(a) Theoretical signatures corresponding to models in (b)

Legend (c): 0.24 V, 0.54 V, 0.70 V, 0.84 V, 1.00 V, 1.15 V

(c)

Pt_6 "clean"
0.54 V = double layer

Pt_6-O(H), 1-fold O(H)$_{ads}$
0.70 – 0.84 V = O$_{ads}$

Pt_6-O, 2-fold O$_{ads}$
1.00 V = 2-fold O$_{ads}$

Pt_6-O$_{ads}$, 3-fold (fcc) O$_{ads}$
0.24 V = 3-fold H$_{ads}$
1.00 V = 3-fold O$_{ads}$

Pt_6-O$_{ads}$, 4-fold (hcp) O$_{ads}$
1.15 V = subsurface O$_{ads}$ = place exchange

(b) Clusters used for theoretical signatures

(d)

Fig. 2. In situ *measurements of XANES and the corresponding Δμ signatures. (a) The theoretical signatures calculated using Janin clusters, shown in (b) and (c), show the corresponding data of experimental Δμ using 0.54 V (vs. RHE) as the clean reference. Note the remarkable similarity between theoretical and experimental profiles. Also shown in (d) is the graphical rendition of the so called "place exchange mechanism."*

structure to the nitrogen-iron chelates in biological heme groups, have been shown to exhibit facile 4e⁻ ORR kinetics at a fraction of the cost of state-of-the-art Pt. Recently we have begun—in collaboration with University of New Mexico (Professor Attanasov's group)—to study a pyrolyzed Co-TMPP-based system via both electrochemical and *in situ* XAS methods. Results[38] to date, shows impressive performance in a PEM fuel cell. Further, analysis of Tafel slopes showed the material to follow the well known- 60/120 mV dec⁻¹ slope relationship in the acid electrolyte with an exchange current density (i_0) of 3×10^{-5} mA cm⁻². While considerably out-performed by Pt-based electrocatalysts, the performance of the Co-TMPP material is quite attractive in light of economic considerations.[39]

Our initial efforts to elucidate the structure/property relationships that give rise to ORR activity of the pyrolyzed Co-TMPP materials via *in situ* XAS are presented in Fig. 3. Three systems (pyrolyzed at 600, 700, and 800°C respectively) were probed at the Co K edge (7709 eV) while under electrochemical control in a 1M TFMSA-flooded electrochemical cell.[40] Analysis of the XANES spectra (Fig. 3b) showed that the Co was in an oxidation state of 2+ for the CoTMPP systems based on a determination of the absorption edge energy compared to Co foil. A full EXAFS analysis of the materials confirmed that the Co-N₄ planar structure (*cf.* Fig. 3a) was maintained (to different extents in
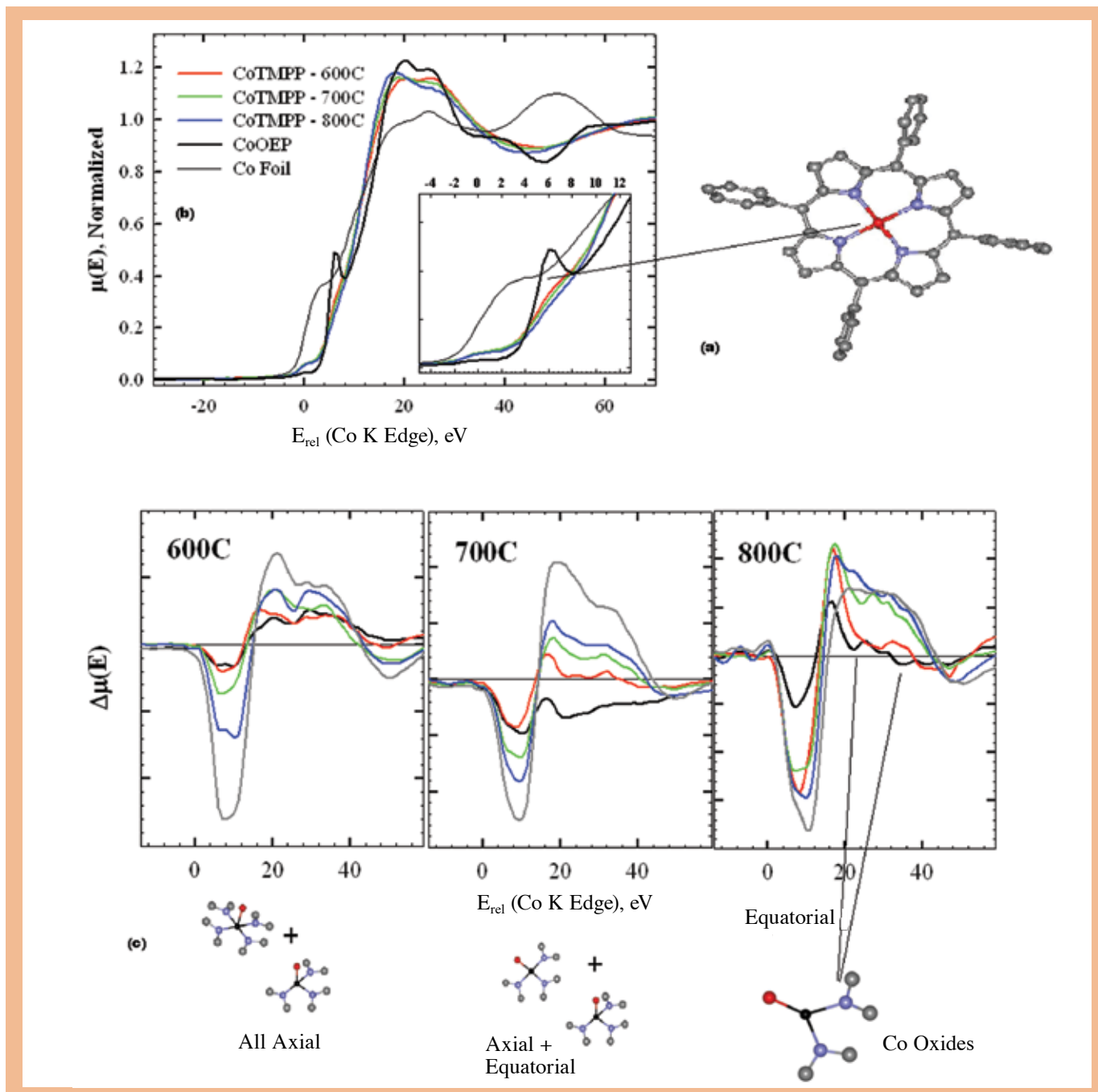

Fig. 3. *Overview of the* in situ *XAS results for pyrolyzed Co-porphyrin electrocatalysts: (a) schematic of a CoTPP molecule with Co in red, N in blue, and C in grey; (b) XANES spectra for the denoted electrocatalysts at 0.40 V in 1M TFMSA electrolyte with an ex situ Co foil added for reference; and (c) the Δμ = μ(V) - μ(0.30 V) spectra for the CoTMPP electrocatalysts pyrolyzed at the noted temperatures (for the Δμ spectra: black = 0.50 V, red = 0.60 V, green = 0.80 V, and blue = 1.00 V). Also shown below are the models to which these experimental signals coincide.*

Mukerjee, *et al.*
(continued from previous page)

relation to the pyrolysis temperature), and avoided the possibility of metallic Co existing in the systems.

The corresponding Δµ spectra (Fig. 3c) were generated with the XANES spectra according to the relation: $\Delta\mu = \mu(V) - \mu(0.30\ V)$, where the 0.30 V anodic potential represents the cleanest, adsorbate-free surface. It is immediately apparent that the resulting spectra, now free of interfering signals from inactive moieties, for the 600°C material differ considerably from the 700 and 800°C analogues. Theoretical FEFF8 calculations[41] based on the central portion of the model in Fig. 3a showed that the double peak feature present only in the 600°C moiety can be attributed to 1-fold O_{ads} normal to the CoN_4 plane. For the 700 and 800°C varieties the sharp drop off after the maximum could only be fit by 1-fold O_{ads} *within* a CoN_3 or CoN_2 plane. Later XPS analysis confirmed that the N:Co ratio was decreasing in respect to higher pyrolysis temperatures.[38] Further, RRDE studies have shown that the overall peroxide yields increase with respect to an increase in pyrolysis temperature. Apparently, removal of one or two of the nitrogen atoms causes O to adsorb in-plane with the Co-N moiety, skewing the ORR mechanism to H_2O_2 formation. Simultaneously, a report was published on density functional theory calculations,[42] which are consistent with the XAS results.

These initial results are incredibly promising. In this case, Δµ analysis was able to indicate not only the nature of the electrocatalyst (CoN_2 vs. CoN_4) and the adsorbed species under real in situ electrochemical operating conditions, but has indicated that a change in the $Co-O_{ads}$ adsorption angle contributes to the production of hydrogen peroxide under ORR conditions. These results are now being refined with more tightly constrained analysis.

Correlating morphology effects on PtRu and direct alcohol oxidation.—Direct methanol oxidation and reformate tolerance represent two very challenging but significantly different electrocatalytic issues. The predominant surface reaction (Langmuir-Hinshelwood type) is poisoning by CO (or similar C_1 moieties), its oxidation occurs via the interaction of CO_{ad} (or C_1 moieties) with surface adsorbed OH_{ad}. Binary catalysts such as PtSn, PtMo, or PtRu offer superior performance but their individual capabilities is a complex function of surface morphologies and the precise nature and distribution of oxide species on the surface. At least three different mechanisms have been proposed, whereby the alloying element[43] (a) modifies the electronic properties of the Pt by contributing d-electron density (the so-called ligand or electronic mechanism); (b) blocks the CO poison formation reaction; or (c) induces co-adsorption of oxygen containing species O(H), which can then take part in the CO oxidation reaction that removes the poison from the surface (the so-called bi-functional mechanism). Although the latter bi-functional mechanism is preferred by a majority of workers in the field, some in situ experimental results, for PtSn for example, suggest that the electronic mechanism is more active,[44,45] and both may be active in some cases.[46-48]

Using a special in situ PEM fuel cell developed to allow *operando* XAS measurements,[49] the structure of a Pt-Ru anode, obtained from EXAFS, and adsorbate coverage, obtained from the Δµ XANES techniques, were followed as a function of the current in either hydrogen or vaporized 1 M methanol solution at elevated temperatures.[32] The objective was to understand differences between various PtRu electrocatalysts prepared using different procedures. The Watanabe method[50] (PtRuW, 1:1 and 3:1) represents a well known procedure to prepare mixed oxides of Pt and Ru, whereas the ETEK derived PtRu (1:1 atomic ratio) (PtRuE) represents the alloy intermetallic state (a fuller characterization is contained in Ref. 51).

Figure 4 shows the relative change of each indicated species determined from the Δµ amplitudes in the shaded regions as shown above at both the Pt L_3 edge and Ru K edge of the PtRu(ETEK) and two different PtRu (Watanabe) samples (3:1 and 1:1 PtRu atomic ratios) at various potentials. Note that in Fig. 4 no attempt was made to include any scale factors to indicate absolute adsorbate coverage, so the plots show only the relative change in adsorbate coverage during the potential cycling, and each adsorbate is on a different scale. CO is observed at both the Ru and Pt surfaces, with a higher amount at the Ru surface. The agreement between these results for CO and that reported previously by Friedrich, *et al.*[52] using *in situ* IR data for Ru/Pt (111) are remarkable, except that the threshold for CO oxidation falls at 0.5 V in Friedrich instead of at 0.28 V as in Fig. 4 clusters compared to Pt (111). The level of detail in figure 4 is remarkable. Note that the coverage of OH generally increases sharply right after the point where CO goes down, thus revealing CO+OH oxidation mechanism, and Fig. 4 further reveals the location of the responsible OH (on the Ru or on the Pt near and away from Ru islands) in the CO oxidation. For the first time it is possible to map the oxidation of species such as CO present on various sites on a bimetallic electrocatalysts surface. The results are significantly different from the PtRu (ETEK) case. CO present at the Pt edge is removed in two distinct regions (from 0 to 0.25 V and from 0.45 to 0.7 V). Accumulation of oxygen on the Pt surface occurs earlier (beginning at 0.35 to 0.4 V) and occurs in the opposite order of the PtRu (ETEK) case; that is atop OH/Pt away from Ru and *n*-fold O/ Pt accumulate first, followed shortly by atop OH/Pt near Ru. Principal oxidation of CO on Pt in PtRu (ETEK) occurs only after ~0.2 V vs. RHE. Whereas in the case of PtRu (Watanabe) two distinct regions, 0 to 0.25 V and 0.4 to 0.6 V. two waves are observed. Details of these data are discussed in Ref. 32.

Summary and Outlook

Biological mimics and enzymes are also being investigated as potential, inexpensive alternatives to precious metal catalysts.[53,54] In short, the use of synchrotron based XAS method remains one of the truly powerful techniques to study charge transfer on transition metal surfaces. The transition from early studies on supported metal clusters such as Pt and Pt alloys is now transitioning into the domain of more complex reaction centers. This was exemplified here by the brief discussion of recent results on Co-porphyrin complex. New results are now emerging on using this technique to understand and then design new metal inorganic framework structures such as Rh_xS_y chalcogenides investigated recently.[37] This is important as in all these systems the individual transition metal atoms are placed in fixed geometries and ligand environments as opposed to classical metal clusters. Our exploration on non-Pt group metals for application in PEM fuel cells will focus on new designs of such complexes and open framework structures. In addition the power of this technique is evident in its ability to provide detailed degradation mechanisms with an unprecedented ability to probe with element specificity, oxide growth, dissolution, surface segregation, and sintering while under actual fuel cell operating mode with control in overpotential, temperature, interfacial water activity (relative humidity in case of PEMFC), etc.　■

References

1. C. Roth, N. Benker, T. Buhrmester, M. Mazurek, M. Loster, H. Fuess, D. C. Koningsberger, D. E. Ramaker, *J. Am. Chem. Soc.*, **127**, (42), 14607 (2005).

2. S. Motoo, M. Watanabe, U.S. Patent 4,797,380, 1989.

3. R. Heck, *Appl. Catal., B: Environ.*, **37**, N6 (2002).

4. A. L. Ankudinov, B. Ravel, J. J. Rehr, and S. D. Conradson, *Phys. Rev. B*, **B58**, 7565 (1998).

5. E. A. Stern, D. E. Sayers, and F. W. Lytle, *Phys. Rev. B: Solid State*, **11**, 4836 (1975).

6. A. E. Russell and A. Rose, *Chem. Rev.*, **104**, 4613 (2004).

7. S. Stoupin, E.-H. Chung, S. Chattopadhyay, C. U. Segre, and E. S. Smotkin, *J. Phys. Chem. B*, **110**, 9932 (2006).

8. R. Viswanathan, G. Hou, R. Liu, S. R. Bare, F. Modica, G. Mickelson, C. U. Segre, N. Leyarovska, and E. S. Smotkin, *J. Phys. Chem. B*, **106**, 3458 (2002).

9. S. Stoupin, H. Rivera, Z. Li, C. U. Segre, C. Korzeniewski, J. Dominick, J. Casadonte, H. Inoue, and E. S. Smotkin, *Phys. Chem. Chem. Phys.*, In press, 2008.

10. S. Mukerjee and J. McBreen, *J. Electroanal. Chem.*, **448**, 163 (1998).

11. H. Yoshitake, O. Yamazaki, and K. Ota, *J. Electrochem. Soc.*, **141**, 2516 (1994).

12. S. Mukerjee, S. Srinivasan, M. P. Soriaga, and J. McBreen, *J. Phys. Chem.*, **99**, 4577 (1995).

13. N. M. Markovic and P. N. Ross, *Surf. Sci. Rep.*, **45**, 117 (2002).

14. M. E. Herron, S. E. Doyle, S. Pizzini, K. J. Roberts, J. Robinson, G. Hards, and F. C. Walsh, *J. Electroanal. Chem.*, **324**, 243 (1992).

15. H. A. Gasteiger, N. M. Markovic, and P. N. Ross, *J. Phys. Chem.*, **99**, 8920 (1995).

16. K. I. Pandya, E. B. Anderson, D. E. Sayers, W. E. O'Grady, *J. Phys. IV*, **7** (C2, Vol. 2), 955 (1997).

17. G. A. Camara, M. J. Giz, V. A. Paganin, and E. A. Ticianelli, *J. Electroanal. Chem.*, **537**, 21 (2002).

18. J. McBreen and S. Mukerjee, *J. Electrochem. Soc.*, **142**, 3399 (1995).

19. P. Piela, C. Eickes, E. Brosha, F. Garzon, and P. Zelenay, *J. Electrochem. Soc.*, **151**, A2053 (2004).

20. B. Shyam, T. Arruda, J. M. Ziegelbauer, S. Mukerjee, and D. E. Ramaker, *ECS Trans.*, **11**, 1, 1359 (2007).

21. D. E. Ramaker and D. C. Koningsberger, *Phys. Rev. Lett.*, **89**, 139701 (2002).

22. D. E. Ramaker, M. Teliska, Y. Zhang, A. Yu, and D. C. Koningsberger, *Phys. Chem. Chem. Phys.*, **5**, 4492 (2003).

23. M. Teliska, W. E. O'Grady, and D. E. Ramaker, *J. Phys. Chem. B*, **108**, 2333 (2004).

24. M. Teliska, D. E. Ramaker, V. Srinivasamurthi, and S. Mukerjee, in *Fundamental Understanding of Electrode Processes in Memory of Professor Ernest B. Yeager*, J. Prakash, et al., Eds., PV2003-30, p. 212, The Electrochemical Society Proceedings Series, Pennington, NJ (2003).

25. M. Teliska, W. E. O'Grady, and D. E. Ramaker, *J. Phys. Chem. B*, **108**, 2333 (2004).

26. J. M. Ziegelbauer, D. Gatewood, A. F. Gulla, D. E. Ramaker, and S. Mukerjee, *Electrochem. Solid-State Lett.*, **9**, A430 (2006).

27. M. Teliska, V. S. Murthi, S. Mukerjee, and D. E. Ramaker, *J. Electrochem. Soc.*, **152**, A2159 (2005).

28. M. Teliska, W. E. O'Grady, and D. E. Ramaker, *J. Phys. Chem. B*, **108**, 2333 (2004).

29. M. Teliska, W. E. O'Grady, and D. E. Ramaker, *J. Phys. Chem. B*, **109**, 8076 (2005).

30. D. E. Ramaker, M. Teliska, Y. Zhang, A. Y. Stakheev, D. C. Koningsberger, *Phys. Chem. Chem. Phys.*, **5**, 4492 (2003).

31. C. Roth, N. Benker, T. Buhrmester, M. Mazurek, M. Loster, H. Fuess, D. C. Koningsberger, and D. E. Ramaker, *J. Am. Chem. Soc.*, **127**, 14607 (2005).

32. F. J. Scott, S. Mukerjee, and D. E. Ramaker, *J. Electrochem. Soc.*, **154**, A396 (2007).

33. M. Teliska, V. S. Murthi, S. Mukerjee, and D. E. Ramaker, *J. Phys. Chem. C*, **111**, 9267 (2007).
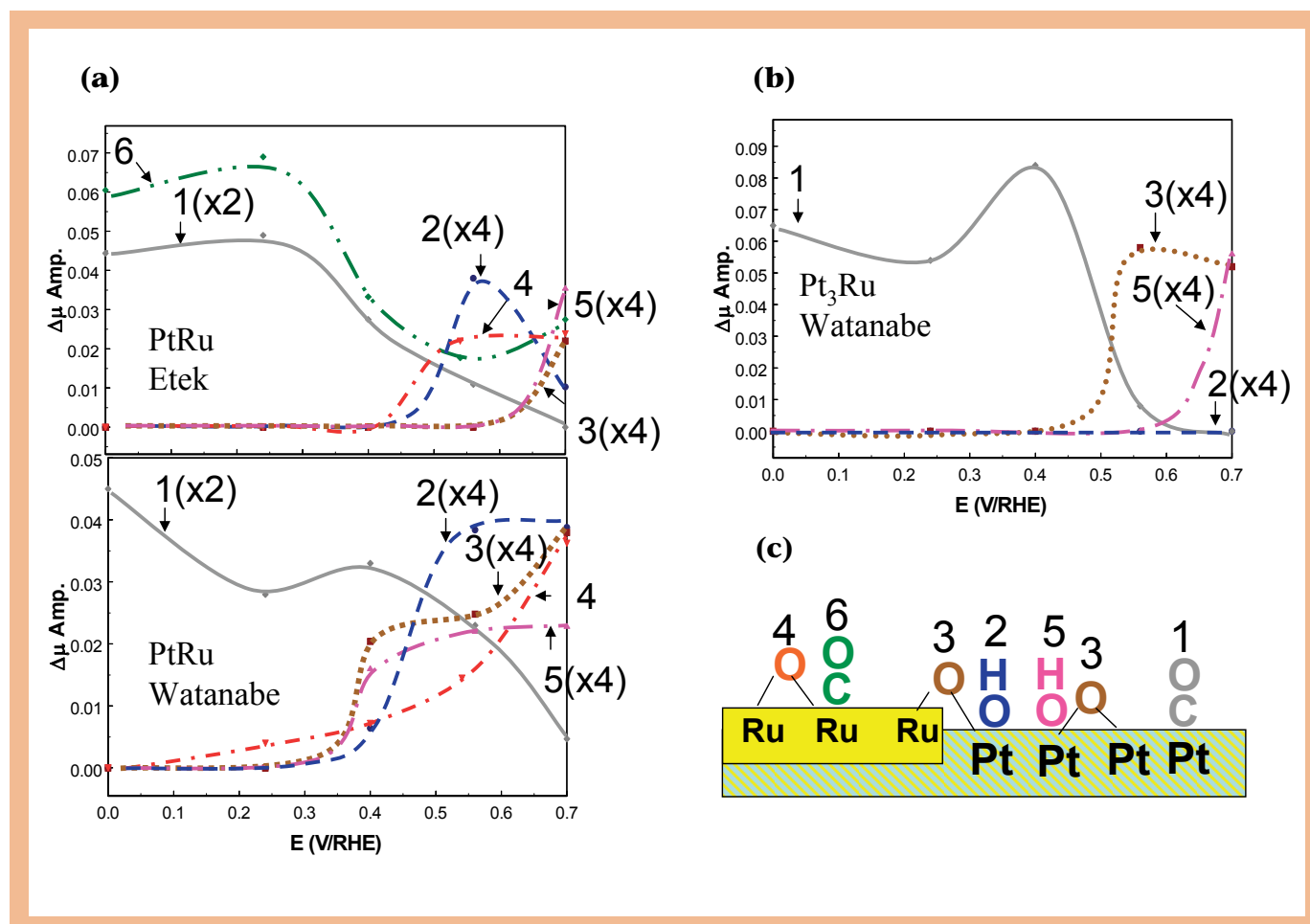
Fig. 4. $\Delta\mu$ *XANES amplitudes for PtRu (ETEK) (a); and PtRu Watanabe (b) and Pt₃Ru Watanabe (c) corresponding to the various adsorbates on Pt and Ru atoms, mapped using* in situ *XANES at the Pt L3 and Ru K edges. More details of this analysis in Ref. 32.*

Mukerjee, *et al.*
(continued from previous page)

34. M. Teliska, W. E. O'Grady, and D. E. Ramaker, *J. Phys. Chem. B*, **109**, 8076 (2005).
35. H. Wroblowa, M. L. B. Rao, A. Damjanovic, J. O'M. Bockris, *J. Electroanal. Chem. Interfacial Electrochem.*, **15**, 139 (1967).
36. A. Damjanovic and V. Brusic, *Electrochim. Acta*, **12**, 1171 (1967).
37. J. M. Ziegelbauer, D. Gatewood, A. F. Gulla, D. E. Ramaker, and S. Mukerjee, *Electrochem. Solid-State Lett.*, **9**, A430 (2006).
38. S. Pylypenko, S. Mukherjee, T. S. Olson, and P. Attanassov, *Electrochim. Acta*, **53**, 7875 (2008).
39. B. Wang, *J. Power Sources*, **152**, 1 (2005).
40. J. M. Ziegelbauer, T. S. Olson, S. Pylpenko, F. Alamgir, C. Jaye, P. Atanassov, and S. Mukerjee, *J. Phys. Chem. C*, **112**, 8839 (2008).
41. A. L. Ankudinov, B. Ravel, J. J. Rehr, and S. D. Conradson, *Phys. Rev. B*, **58**, 7565 (1998).
42. E. Vayner and A. B. Anderson, *J. Phys. Chem. C*, **111**, 9330 (2007).
43. B. R. Rauhe, Jr., F. R. McLarnon, and E. J. Cairns, *J. Electrochem. Soc.*, **142**, 1073 (1995).
44. S. Mukerjee and J. McBreen, *J. Electrochem. Soc.*, **146**, 600 (1999).
45. H. A. Gasteiger, N. M. Markovic, and P. N. Ross, *Book of Abstracts, 210th ACS National Meeting, Chicago, IL*, August 20-24, 1995, (Pt. 1), INOR-296.
46. G. Samjeske, X. Y. Xiao, and H. Baltrushat, *Langmuir*, **18**, 4659 (2002).
47. H. W. Kei, S. Suh, B. Gurau, B. Workie, R. X. Liu, and E. S. Smotkin, *Electrochim. Acta*, **47**, 2913 (2002).
48. C. Lu, I. C. Lee, R. I. Masel, A. Wieckowski, and C. Rice, *J. Phys. Chem. A*, **106**, 3084 (2002).
49. C. Roth, N. Benker, T. Buhrmester, M. Mazurek, M. Loster, H. Fuess, D. C. Koningsberger, and D. E. Ramaker, *J. Am. Chem. Soc.*, **127**, (42), 14607 (2005).
50. M. Watanabe and S. Motoo, U.S. Patent 4,797,380, 1989.
51. F. J. Scott, S. Mukerjee, and D. E. Ramaker, *J. Electrochem. Soc.*, **154**, A396 (2007).
52. K. A. Friedrich, P. P. Geyser, U. Linke, U. Stimming, and L. Stumper, *J. Electroanal. Chem.*, **402**, 123 (1996).
53. C. J. Chang, L. Zhi-Heng, C. Shi, F. C. Anson, and D. C. Nocera, *J. Am. Chem. Soc.*, **126**, 10013 (2004).
54. B. Wang, *J. Power Sources*, **152**, 1 (2005).

About the Authors

SANJEEV MUKERJEE is a professor in the Department of Chemistry and Chemical Biology, Northeastern University, Boston, and Director of the Center for Renewable Energy Technology. During the last 18 years, he has focused on understanding charge transfer processes at electrochemical interfaces to elucidate electrocatalytic pathways and intercalation phenomenon. These have lead to significant advances in our understanding of structure property relationships on Pt and Pt alloy electrocatalysts for PEM applications as well as the development of new materials with enhanced stability, activity, and selectivity. In these endeavors, the use of *in situ* synchrotron X-ray spectroscopy (absorption and scattering) have been pioneered starting from early '90s to the current rendition enabling the determination of surface adsorbed states. He may be contacted at s.mukerjee@neu.edu.

JOSEPH ZEIGELBAUER is currently a project engineer at General Motors Central Research in Warren, Michigan. His interests are in electrocatalysis and corrosion. As a graduate student in Professor Mukerjee's group, he laid the foundation of applying the new rendition of the X-ray absorption spectroscopy to complex metal framework structures in order to identify the reaction center and electrocatalytic pathways. He is also an avid musician and may be contacted at joseph.ziegelbauer@gm.com.

THOMAS ARRUDA, currently a senior level graduate student in Professor Mukerjee's group, is spear-heading the understanding of electron transfer in mediated and unmediated enzymatic reaction centers for biological fuel cell applications. He also enjoys sailing and brewing in his spare time. He may be contacted at arruda.t@neu.edu.

DAVID RAMAKER is a professor in the Department of Chemistry, and Director of the Institute for Materials Science, at George Washington University, along with a part-time appointment at the Naval Research Lab. He is a Fellow in the American Vacuum Society and the Washington Academy of Sciences, and is a member of ECS. He and his research group have developed new *in situ* techniques in X-ray absorption spectroscopy. He may be reached at ramaker@gwu.edu.

BADRI SHYAM is a fourth year graduate student at George Washington University. At GWU he is developing and applying X-ray absorption spectroscopy analysis techniques to a wide range of fuel cell and electrocatalyst problems to enable the determination of atomic adsorption sites on small metal particles used as electrocatalysts in PEM fuel cells. He is huge Bob Dylan fan and also a wizard with guitars, and may be reached at badri@gwu.edu.